Lab on a Chip

PAPER

View Article Online
View Journal | View Issue

Cite this: *Lab Chip*, 2018, **18**, 522

A fluorescent microbead-based microfluidic immunoassay chip for immune cell cytokine secretion quantification†

Xin Cui,‡[ab] Ya Liu,‡[a] Dinglong Hu,[a] Weiyi Qian,[b] Chung Tin,[acde] Dong Sun,[ac] Weiqiang Chen *[b] and Raymond H. W. Lam *[acde]

Quantitative and dynamic analyses of immune cell secretory cytokines are essential for precise determination and characterization of the "immune phenotype" of patients for clinical diagnosis and treatment of immune-related diseases. Although multiple methods including the enzyme-linked immunosorbent assay (ELISA) have been applied for cytokine detection, such measurements remain very challenging in real-time, high-throughput, and high-sensitivity immune cell analysis. In this paper, we report a highly integrated microfluidic device that allows for on-chip isolation, culture, and stimulation, as well as sensitive and dynamic cytokine profiling of immune cells. Such a microfluidic sensing chip is integrated with cytometric fluorescent microbeads for real-time and multiplexed monitoring of immune cell cytokine secretion dynamics, consuming a relatively small extracted sample volume (160 nl) without interrupting the immune cell culture. Furthermore, it is integrated with a Taylor dispersion-based mixing unit in each detection chamber that shortens the immunoassay period down to less than 30 minutes. We demonstrate the profiling of multiple pro-inflammatory cytokine secretions (*e.g.* interleukin-6, interleukin-8, and tumor necrosis factors) of human peripheral blood mononuclear cells (PBMCs) with a sensitivity of 20 pg ml^{-1} and a sample volume of 160 nl per detection. Further applications of this automated, rapid, and high-throughput microfluidic immunophenotyping platform can help unleash the mechanisms of systemic immune responses, and enable efficient assessments of the pathologic immune status for clinical diagnosis and immune therapy.

Received 6th November 2017,
Accepted 2nd January 2018

DOI: 10.1039/c7lc01183k

rsc.li/loc

Introduction

The immune system is the defense mechanism that protects living organisms from being invaded by viruses, bacteria, and parasitic worms, by distinguishing pathogens and diseased tissues from healthy cells and tissues and eliminating them. However, it is still a significant clinical challenge to accurately diagnose and efficiently treat immune and infectious diseases due to the cellular functional heterogeneity of patient samples and the highly dynamic nature of disease development.[1,2] In order to tackle this challenge, a close monitoring of the functions of our immune defense unit – leukocytes (immune cells), which play a major role in innate and adaptive immune responses,[3,4] has to be performed. Leukocytes orchestrate immune responses by releasing various essential cell signaling biomolecules known as cytokines.[5] The cytokine secretion profiles of different subtypes of immune cells are spatiotemporally regulated for host defense against viral or bacterial infections, intracellular interactions, and inflammation responses.[6] For example, leukocytes secrete multiple cytokines functioning as mediators and modulators of inflammatory responses. Pro-inflammatory cytokines such as interleukin (IL)-6 and IL-8 are secreted in the early stage of immune diseases, which can be restored by anti-inflammatory cytokines, such as IL-10 and tumor necrosis factor (TGF)-β to obtain the homeostasis of immune systems.[7,8] Given the heterogeneity and dynamic behaviors of different leukocyte subpopulations, an accurate, quantitative, and multiplexed cytokine measurement is required and essential for functional characterization of immune cell phenotypes of patients for clinical diagnosis of immune-related diseases.[9]

Up to now, cytokine measurements have been largely conducted with the conventional enzyme-linked

[a] *Department of Mechanical and Biomedical Engineering, City University of Hong Kong, Hong Kong. E-mail: rhwlam@cityu.edu.hk; Fax: +852 3442 0172; Tel: +852 3442 8577*
[b] *Department of Mechanical and Aerospace Engineering, New York University, NY, USA. E-mail: wchen@nyu.edu; Fax: +1 646 997 3136; Tel: +1 646 997 3767*
[c] *Centre for Robotics and Automation, City University of Hong Kong, Hong Kong*
[d] *Centre for Biosystems, Neuroscience, and Nanotechnology, City University of Hong Kong, Hong Kong*
[e] *City University of Hong Kong Shenzhen Research Institute, Shenzhen, China*
† Electronic supplementary information (ESI) available. See DOI: 10.1039/c7lc01183k
‡ These authors contributed equally to this work.

immunosorbent assay/spot[10] (ELISA/ELISpot) on plate readers or the cytometric bead-based immunoassay using flow cytometry.[11,12] However, it remains challenging to achieve real-time, multiplex and sample-sparing cytokine profiling using conventional immunophenotyping methods.[13] Such a challenge is largely caused by the short period of immune status transition (as short as several hours) and limited supply of blood samples from patients (particularly pediatric patients).[13–15] Development of sample-sparing assays will lead to more efficient use of the sample materials through a significant reduction of sample volumes or by simultaneous, multi-parameter assessments of immune functions. Furthermore, the inherent laborious, time and reagent/biosample-consuming procedures involved in conventional immunophenotyping methods also limit these assays for practical use in clinical settings.[13–15] Continuing progress in many fields, ranging from fundamental biological and clinical discovery to patient care, hinges upon the availability of specific, reliable, and sample-sparing assay systems for multiplex and spatiotemporal cytokine detection.[16,17] Moreover, achieving an integrated, rapid, and sample-efficient assay on blood or cell samples all in one chip would be even more challenging. Hence, there is a great demand for an integrated, rapid, and accurate functional immune cell phenotyping and cytokine detection assays, which may provide important insights into immune-related diseases including autoimmune diseases,[18] infections,[19] chronic inflammation, and cancer.[20]

One challenge in sensitive and rapid optical-immunophenotyping using microfluidic technology is to achieve effective "lab-on-a-chip" bio-reagent processing and mixing.[21,22] While many pioneering micro-devices have been demonstrated as promising immune-monitoring technologies for achieving analysis of cell-secreted molecules, most of these devices still require off-chip purification and stimulation of the target cells from blood prior to analysis.[3,23,24] This necessitates a new integrated approach that would simplify the processes required to isolate, culture, and stimulate target immune cell subsets from biosamples, as well as profile the cell-secreted cytokines from these isolated cells. However, such an integrated lab-on-a-chip system for functional cellular immunophenotyping is largely missing.[13] In addition to the on-chip cell isolation and manipulation,[25] subsequent bio-reagent processing and mixing are also essential to the sensing performance.[21,22] In order to enhance the sensor detection sensitivity, the majority of previous effort has been focused on the sensor materials and sensing mechanisms. Optimization of transportation and mixing of target molecules in a confined microenvironment is largely overlooked. Indeed, it has been shown that biomolecule transportation also plays a critical role in governing binding kinetics and ultimately sensor performance.[26] Yet, most of the current sensing systems rely upon pure analyte diffusion, which limits both the detection sensitivity and speed (hours to days).[27] Therefore, new methods that can shift the analyte binding mechanism from passive diffusion to an active, hydrodynamic biomolecule transportation and condensing process will break the current system limits and further enhance the sensing performance. Although many passive,[28] continuous-flow micromixers[29] such as flow-focusing[30] and microstructured channel walls[31] have been developed to reduce the characteristic mixing length by disturbing the laminar flow in a confined space, mixing of different reagents in an extremely small sample volume (micro- to nano-liter level) and a precise volume ratio for immunoassays remains challenging.[13]

Active mixing with a spatial-periodic alternating flow within a confined microchannel or microchamber offers a consistent and precise volume ratio of reagents, which can fulfill the high efficiency and repeatability requirements for immunoassays. For example, Chou *et al.* invented an active mixing scheme along an isolated rotary microchannel based on Taylor dispersion[32] driven by pneumatic micropumps[33] and demonstrated a nearly two orders of magnitude enhancement of surface-binding assay. Recently, Junkin *et al.* applied an active mixing scheme and determined the dynamics of single immune cells in an automated high-throughput microfluidic chip.[34] However, the reported mixing period was >1 h for a stable fluorescence intensity, which may limit the real-time profiling of cytokine dynamics. Using a diaphragm actuator and integrating micro-pillar structures in their microfluidic device, Lam and Li could achieve a high-throughput and rapid fluid mixing (5 s for liquid outflow >1 mL min^{-1}) for biological assays.[35] Further, a rotating impeller has been developed recently to effectively mix a wide range of yield stress fluids with a gap size on the order of hundreds of micrometers, demonstrating microfluidic active mixers for mixing complex fluids at the microscale.[36] Our recent study also demonstrated an active micromixer by generating circulation flows in an enclosed microchamber to shorten the mixing time by ~10 times.[37] These active micromixers provide rational frameworks to design on-chip mixing units for efficient and accurate cytokine detection.[38]

In the past decade, a number of microfluidic techniques have been developed for the quantitative measurements of cytokine secretions.[39,40] These microfluidic detection methods include immunofluorescence staining,[41] chemiluminescence,[42] nanoparticle deposition,[43] localized surface plasmon resonance,[44] quartz crystal microbalance,[45] and magnetoelectronic detection[46] which show the capabilities of high-throughput analysis, low reagent consumption, automated fluid handling, and process integration. Among these microfluidic sensing techniques, optical detection schemes are widely adopted due to the ease of integration of many existing fluorescently-labeled bio-reagents and optical microscopy with transparent microfluidic systems for optical imaging. In particular, a multiplexed bead-based immunoassay with its increased surface-to-volume ratio, convenient fluid transporting, and enhanced flexibility for detecting cytokine subpopulations[39,47,48] is an attractive technique to be used for an on-chip multiplex detection of cytokine secretion dynamics[48,49] for medical diagnosis.

Here, we report an integrated microfluidic immunoassay device that allows on-chip immune cell isolation, culture, biochemical stimulation, and biosample processing, as well as downstream dynamic profiling of multiple cytokine secretions

using a micro-liter volume of samples. The immunoassay device contains three main components: a cell culture chamber, an array of cytokine detection units and an array of active peristaltic mixers for on-chip sample mixing. The cell culture chamber supports cell isolation, culture, and biochemical stimulation in the microfluidic environment. The detection microchambers loaded with clinically adopted[50,51] cytometric fluorescent beads are designed for a multiplex and dynamic cytokine measurement. Each detection chamber is integrated with an active circulating flow micro-mixer with precisely defined mixing ratios, such that the required volume of biosamples (*e.g.* blood extracts) per detection is significantly reduced (from ~3 ml to 0.5 μl) and the detection period can be shortened to less than 30 minutes. As a demonstration, we applied this immunoassay device to characterize peripheral blood mononuclear cells (PBMCs) for their dynamic immunoresponses upon inflammatory phytohaemagglutinin (PHA) stimulation. This integrated immunoassay platform can be potentially applied for an accurate immunophenotyping of the pathologic immune status of patients, unveiling biological mechanisms of immune-related diseases, and facilitating personalized immunotherapy for immune diseases and cancer.[52,53]

Materials and methods

Fabrication

The microfluidic device fabrication was based on replica molding of polydimethylsiloxane (PDMS; Sylgard-184, Dow

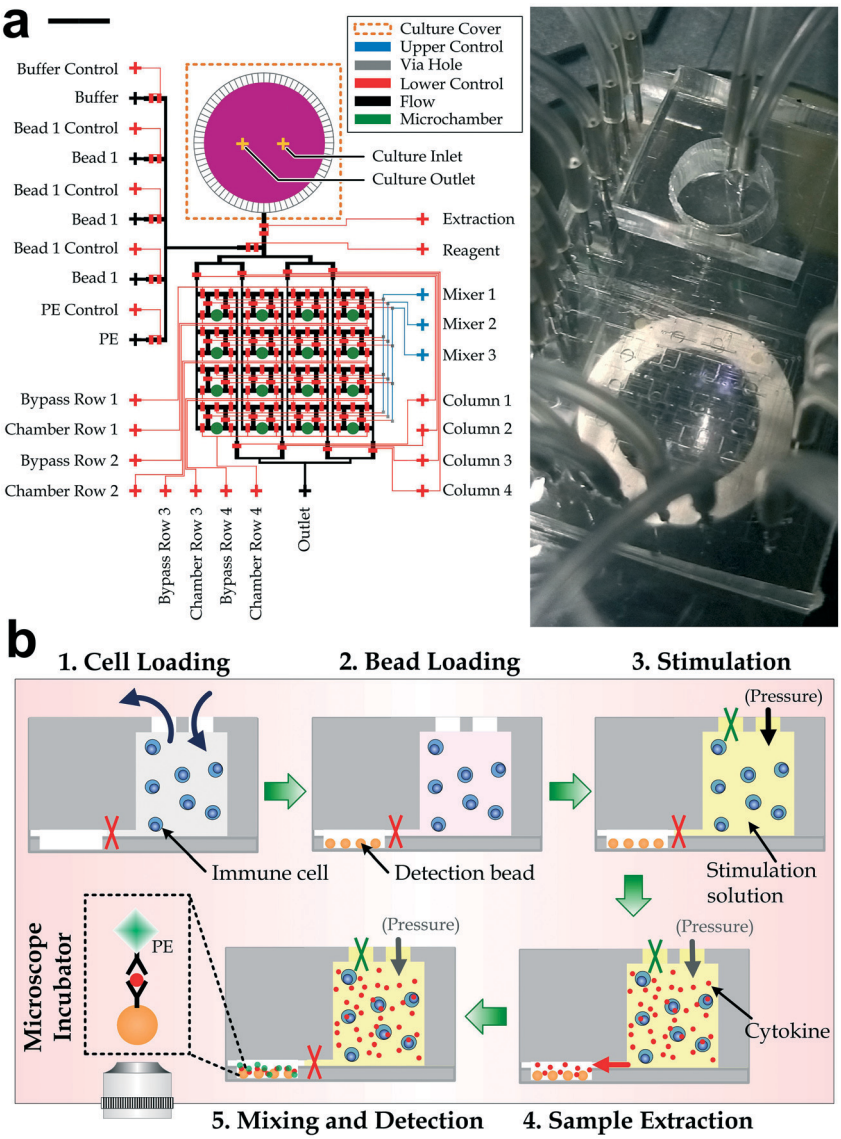

Fig. 1 Design and operation of the microfluidic immunoassay device. (a) Layout (left) and photograph (right) of the device. Scale bar: 4 mm. (b) Cell culture, stimulation and cytokine detection procedures: 1) load and incubate immune cells in the device placed in the microscope incubator at 37 °C and 5% CO_2; 2) load detection beads sequentially into each of the detection chambers, 2) stimulate immune cells with the culture chamber closed (green cross) afterward; 4) extract a small portion of the cytokine-containing culture media to a detection chamber; and 5) mix, incubate and wash the cytokine-sensitive beads and quantifying the fluorescence intensities under a microscope.

Corning) as described in Fig. S1.† Three molds were first fabricated by photolithography of SU-8 photoresist (SU-8100, Microchem) on silicon wafers for the microchannels in the upper control layer (height: 20 μm), the lower control layer (height: 20 μm for the gas channels and 100 μm for the via-holes) and the chamber layer (height: 500 μm) contained in the microfluidic device (Fig. 1a). The flow layer of the microfluidic device (Fig. 1a) was photolithographically patterned with the SU-8 photoresist (SU-8 2005 Microchem) for the cell culture region (height: ~1 μm) and the AZ50XT photoresist (AZ Electronic Materials) with reflow at 120 °C for 1 min for the remaining flow microchannels (thickness: 20 μm). After these molds were fabricated, the mold surfaces were salinized with trichloro(1*H*,1*H*,2*H*,2*H*-perfluoro-octyl)silane (Sigma-Aldrich) for facilitating the release of the molded PDMS layers in the later procedures.

The microfluidic device was then fabricated by replica molding of PDMS with a 10 : 1 ratio between the prepolymer and hardener, with procedures based on the standard multilayer soft lithography.[33] The thicknesses of the PDMS substrates were: 5 mm for the upper control-layer, 120 μm for the lower control layer, 35 μm for the flow layer and 1 mm for the chamber-layer. In particular, the lower control layer containing via holes was fabricated by curing the PDMS sandwiched between the mold and an overhead polyester surface that can squeeze away the PDMS above the via-hole regions, as we reported previously.[54] After the all the PDMS structure layers were fabricated, the four PDMS layers were then aligned under a stereomicroscope and bonded in sequence after surface air plasma treatments (energy 10 kJ; Harrick plasma cleaner PDC-002). Hole punchers were applied on the PDMS layers for the culture chamber (diameter: 6 mm; WHAWB100082, Sigma-Aldrich) and the gas/liquid inlets and outlets (diameter: 1 mm; WHAWB100073, Sigma-Aldrich). The chamber cover was fabricated in another PDMS layer (thickness: 5 mm) with two holes punched for the biosample inlet and outlet. Using the oxygen plasma treatment, the chamber cover was bonded to the microchamber region; and then the entire stacked PDMS device was bonded to a glass slide (Cytoglass, Nanjing, China) for physical support.

Cell culture

Peripheral blood mononuclear cells (PBMCs; PCS-800-011, ATCC) were cultured in complete RPMI-1640 culture medium supplemented with 10% fetal bovine serum and 1% penicillin in a 37 °C incubator (HERA cell 150, Hereaus, Langenese, Germany) with a humidified and 5% CO_2 environment. PBMCs were thawed and incubated for 2–3 days before experiments in order to ensure the proper cell viability and behaviors.

Flow cytometry-based immunoassay

A commercial human inflammatory cytokine kit (Catalog No. 551811, BD Biosciences) was chosen to quantify cytokine concentrations in the cell samples. Multiple fluorescent microbeads (emission wavelength: 647 nm) specifically captured different cytokines. Notably, ~1000 detection beads were used in each test. After mixing the microbeads with the cytokine samples, the mixture was incubated with a phycoerythrin (PE)-conjugated (emission wavelength: 488 nm) detection antibody reagent for 3 h at room temperature; and the PE fluorescence intensities on the microbeads could then reflect the concentrations of the bound cytokines. Phosphate buffered saline (PBS) was applied as a wash buffer to remove the unbind PE molecules for improving the signal-to-background ratio. Afterward, through the analysis of flow cytometry (Accuri C6 Plus, BD Biosciences, CA, USA), the APC (647 nm) and PE (488 nm) channels were utilized to distinguish different cytokine types and measure the fluorescence intensity of a targeted cytokine, which then was converted to the cytokine level by using a calibration curve between the bead fluorescence intensities and known concentrations of each selected cytokine (5–5000 pg ml^{-1}).

Automated microscope platform

In order to perform the required microfluidic manipulation, cell seeding, stimulation and bead fluorescence intensity detection, we established an automated platform with an inverted microscope (TE300, Nikon, Tokyo, Japan) installed with a microscope camera (Zyla 4.2, Andor, Belfast, UK).[54] The microfluidic device was placed in a confining shield mounted on the microscope stage offering cell incubation with stable temperature (37 °C), humidity and gas (5% CO_2) conditions.

Device preparation and cell seeding

Sterilization of the microfluidic device was achieved by baking at 100 °C for >10 h and applying UV exposure for >2 h. Syringe tubing (Tygon® tubing, US Plastics, Lima, OH) was then connected to the device and filled with distilled water (Fig. 1a) and the computer-controlled pressure supplies (pressure: 0 or 12 psi). Distilled water was then filled into all the control channels, and culture media into all the flow channels and microchambers. Similarly, syringe tubing was also connected to the liquid inlets and filled with the corresponding inlet solutions: phycoerythrin-labeled antibody, detection beads, and a wash buffer (Fig. 1a) with the pressure supplies (pressure: 0 or 0.2 psi). All the control valves except 'Mixer 1' were maintained with a pressure of 12 psi such that all the flow channels and detection chambers were gated by the microvalves. The device then located in the automated microscope platform throughout experimental processes. After a pre-incubation for 30 min at 37 °C and 5% CO_2 under stabilized culture medium conditions, PBMCs (cell density: 3×10^5 cells per ml) were then seeded into the culture chamber through the chamber inlet, followed by maintaining an inlet pressure of 0.2 psi and closing the chamber outlet tubing with a paper clip.

Quantification of single bead intensity for on-chip cytokine detection

A custom Matlab program (Mathworks, Natick, MA) was used to quantify the fluorescence intensity of each microbead for cytokine detection in the microfluidic device. In each measurement, two fluorescence microscopic images were captured by the microscope camera to help label the bead body (647 nm) and quantify the cytokine concentration (488 nm). The bead boundary image was extracted based on the intensity-thresholding and boundary extraction. Next, the average cytokine-representing intensity over the bead regions for each detection bead was quantified in the cytokine microscopic image. Subsequently, such average intensity could then be converted to the concentration of a targeted cytokine based on a calibration curve predetermined by experiments.

Statistics

All experiments were conducted with at least 3 independent experiments. *p*-Values were calculated using Student's *t*-test in Excel (Microsoft), with $p < 0.05$ considered as statistically significant.

Results and discussion

Device design and operation

An integrated microfluidic immunoassay device (Fig. 1) was designed for parallel monitoring of immune cell secretory cytokines under a fluorescence microscope. As shown in Fig. 1a, the immunoassay device contains three main components: a cell culture chamber (*purple*), an array (4 rows × 4 columns) of cytokine detection units (*green*) and an array of active peristaltic mixers. The cell culture chamber (volume: 0.39 ml) supports cell culture and biochemical stimulation in the microfluidic environment. It is surrounded by multiple valve-controlled microchannels connected to the downstream cytokine detection units. Since the height of the microchannel (~1 μm) is designed to be smaller than the diameter of blood cells,[55] these connecting microchannels allow liquid sample transportation while simultaneously trapping the cells in the culture chamber. Each cytokine detection unit consists of a detection chamber (volume: 160 nl) and a bypass channel (volume: 30 nl) containing three peristaltic microvalves[54,56] for active pumping and mixing. The detection chamber stores extracted samples, detection microbeads and other reagents. The peristaltic microvalves can then create a recirculating flow along the detection unit and mix reagents based on the Taylor dispersion effect.[57]

When in operation (Fig. 1b), immune cells are first loaded into the cell culture chamber with open 'Culture Inlet' and 'Culture Outlet' (step 1), while fluorescent detection microbeads are loaded into each detection chamber by releasing the 'Reagent' valve and the inlet control valve for the selected microbead and the pair of 'Chamber Row' and 'Column' valves for the target detection chamber (step 2). Next, cell stimulation molecules are loaded into the culture chamber and the whole device is incubated in the microscope-associated incubator at a stabilized temperature at 37 °C for 2 h to let the immune cells secrete cytokines. During this incubation period, the culture chamber outlet is clamped while the inlet is connected to tubes filled with fresh culture media under a switchable compressed air source (pressure: 0.2 psi) (step 3).

At defined time points during the stimulation period, the compressed air source is switched on and the device microvalves ('Extraction', a selected one of 'Chamber Row' and a selected one of 'Column') are released for 14 s in order to drive a small portion (~0.5 μl) of the sample from the culture chamber to the microbead-containing cytokine detection microchamber (volume: 0.16 μl) for cytokine detection (step 4). Notably, we have arranged the connecting microchannel layout as we previously reported[54,58] such that the channel length from the culture chamber to any of the detection chambers and the corresponding flow condition is identical. Once the detection chamber is filled, all the microvalves should return to the original states to continue the immune cell incubation.

For each cytokine detection, a phycoerythrin-conjugated antibody (PE) solution is loaded along the bypass channels next to the identified detection chamber by controlling the microvalves 'Reagents', 'PE', a selected 'Bypass Row' and a selected 'Column'. Next, the PE solution, the microbeads, and the biosample extract are actively mixed by the peristaltic mixer (step 5). The detection chamber is then flushed with a wash buffer (PBS) for 2 min; and a fluorescence image (488 nm) is captured at the detection chamber for quantification of the cytokine concentration (see Materials and methods for details).

Cell trapping and viability in the culture chamber

The immune cells incubated in the culture chamber of the microfluidic immunoassay device should be maintained under suitable environmental conditions (*e.g.* a sufficiently low hydrostatic pressure[59]) for the functional immune cell cytokine secretion analysis. To examine cell viability in the device, we loaded PBMCs (~3×10^5 cells, occupying about 90% of the culture chamber area) and applied a low pressure (0.2 psi) in the cell culture chamber, to support flow in the media extraction step. Another device without applied pressure in the cell culture chamber was considered as control. We incubated the cells in the devices for 24 h and then performed a cell viability staining assay (cat# L3244, Thermo Fisher Scientific) to examine the cell viability under a fluorescence microscope (TE300, Nikon, Tokyo, Japan). Our results (Fig. 2a) demonstrated comparable cell viability (89% ± SE 1.1% without pressure *versus* 88% ± SE 0.9% with pressure obtained from >5 repeated tests). This proves that cell viability is not compromised by the driving pressure applied in our devices.

It is reported that immune cells with a diameter of 5–10 μm can deform and penetrate into microchannels with

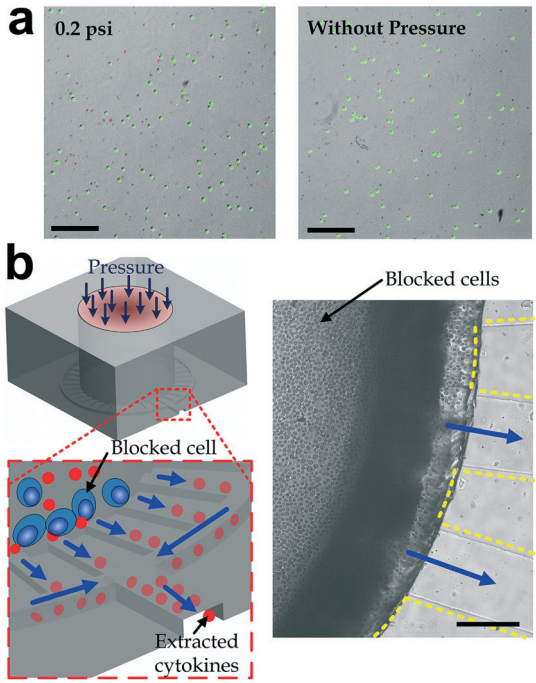

Fig. 2 Trapping and viability of cells in the culture chamber. (a) Bright-field micrographs of stained live (green) and dead (red) cells growing in the culture chamber for 24 h with and without a pressure of 0.2 psi. Scale bar: 50 μm. (b) Drawing (left) and micrograph (right) showing cells maintained in the culture chamber when the sample extraction channel is opened. Blue arrows indicate the media flow directions. Scale bar: 100 μm.

smaller sizes, driven by a hydraulic pressure.[60] In order to prevent such unwanted cell penetration, we designed the heights of the microchannels surrounding the cell culture chamber to be as small as 1 μm. We performed experiments to confirm the cell trapping in the culture chamber under the selected driving pressure of 0.2 psi for 10 min and observed that all cells were maintained in the culture chamber without squeezing into the surrounding microchannels (Fig. 2b).

Sample extraction and mixing

First, we quantified the consistency of the sample extraction flow rate of the reported device as a function of the driving pressure, ranging from 0–0.3 psi, visualized by applying fluorescent-microbeads (diameter: 0.52 μm) flowing along the 'Extraction' microchannel (Fig. S2a†). The flow rates for different driving pressures can then be measured along the extraction microchannel in the device. Considering that a driving pressure of 0.2 psi would induce a flow rate of 27.72 nl s^{-1}, we configured the extraction valve to open for 14 s such that the extracted media would be sufficient to fill up the detection microchamber (volume: 160 nl) in every cytokine measurement. In addition, the total volume used for the array of 4 × 4 chambers from the cell culture chamber was <7.5 μL, which is <2% of the volume of the cell culture chamber. This indicates that there is no significant disturbance caused by changes in molecular concentrations in the cell culture.

We characterized the mixing performance in a detection unit following the procedures described previously, except that a known concentration (625 pg ml^{-1}) of cytokine solution instead of a cell culture was loaded into the culture chamber. Fig. 3a demonstrates the liquid/microbead loading and mixing procedures during device operation, with fluorescent microbeads, *green* and *purple* dye solutions as substitutes for cytokine-sensitive detection microbeads, media extracts and the PE solution, respectively. A higher bead concentration (6 × 10^6 beads per ml) was applied here for visualizing better the spatial distribution of microbead

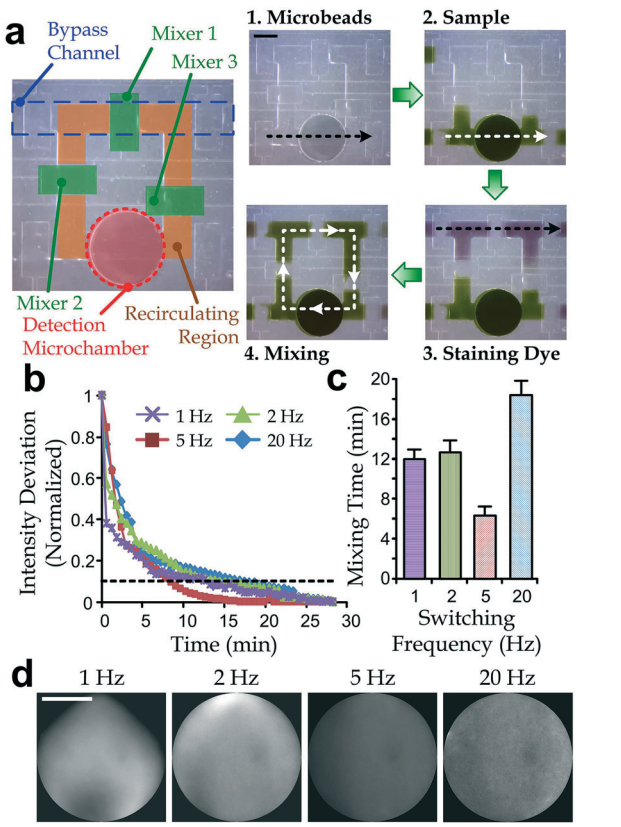

Fig. 3 Characterization of mixing in a cytokine detection region. (a) Demonstration of the mixing operation. The mixing is based on a recirculating flow along the detection microchamber and the recirculating region by peristaltic pumping with the 3 mixer microvalves (left). The cytokine measurement includes four major procedures (right): 1) loading of detection microbeads, 2) insertion of a media extract (green), 3) loading of the PE fluorescent dye along the bypass channel, and 4) mixing of all components such that the PE molecules can stain cytokines bound on the bead surfaces. Scale bar: 400 μm. (b) Standard deviations of fluorescence intensities in the detection chamber region, normalized with the initial deviation before mixing as '1'. The mixing time is defined as the moment when the intensity deviation reached 0.1 for each switching frequency. (c) Mixing time *versus* microvalve switching frequency during mixing. Error bars are standard deviations from 5 repeated experiments of the same frequency. (d) Fluorescence micrographs at the detection chamber after mixing for 10 min with switching times of 1 Hz, 2 Hz, 5 Hz and 20 Hz. Scale bar: 400 μm.

intensities. The device mixed all the components in the detection microchamber and the recirculating channel region by peristaltic pumping using the three mixer microvalves followed by flushing the detection chamber with PBS for 2 min to remove the unbound PE solution.

We then studied if the valve switching frequency would affect the mixing efficiency. In the experiments, the mixing procedures were repeated with different mixer valve switching frequencies (1 Hz, 2 Hz, 5 Hz and 20 Hz) during the mixing process. We defined the mixing efficiency as the standard deviations of the fluorescence intensity[37] over the detection microchamber and the recirculation region: a smaller deviation corresponds to more consistent intensities and a better mixing performance. We further defined the 'mixing time' as the moment when the intensity deviation was reduced to 10% of the maximum value during mixing. The results (Fig. 3b–d) indicate that while all the mixing can achieve sufficient mixing performance after 20 min, the 5 Hz valve switching frequency induced the fastest (mixing time: 6 ± SD 1 min) and most efficient mixing. Therefore, we adopted the switching frequency of 5 Hz and the duration of 10 min for the actual mixing operation in our experiments.

Cytokine measurements in the microfluidic immunoassay device

We calibrated the detection of different concentrations of three key pro-inflammatory cytokines that are related to immune diseases and cancer: IL-6, IL-8 and TNF. In these experiments, cytokine solutions were prepared with eight different concentrations (5000 pg ml^{-1}, 2500 pg ml^{-1}, 1250 pg ml^{-1}, 625 pg ml^{-1}, 312.5 pg ml^{-1}, 156 pg ml^{-1}, 40 pg ml^{-1}, and 20 pg ml^{-1}) by diluting a standard solution (concentration: 5 ng ml^{-1}) with PBS for each of the selected cytokines. About 100 microbeads was loaded in each detection microchamber for targeted cytokine detection. Fluorescence micrographs were taken for the bead bodies (647 nm) and cytokine-sensitive intensities (488 nm) as shown in Fig. 4a, and used to quantify cytokine concentrations based on the fluorescence intensities of microbeads as mentioned in Materials and methods. The calibration curves (Fig. 4b) of IL-6, IL-8 and TNF ranging from 20 pg ml^{-1} to 5000 pg ml^{-1} indicate a good linearity between the bead fluorescence intensity and the cytokine concentration ($R^2 > 0.95$). Our calibration curve further indicates that our fluorescent bead-based cytokine detection can achieve a sensitivity of 20 pg ml^{-1}, which is comparable to the gold standard methods ELISA and flow cytometry.

Profiling cytokine dynamics of PBMCs

We then demonstrate the capability of the microfluidic immunoassay device for functional cytokine dynamics profiling of PBMCs stimulated by phytohaemagglutinin (PHA; cat# L11270, Thermo fisher). PHA is a well-known signaling molecule that is used to induce immune cell inflammation responses. In the live cell experiments, we profiled cytokine dynamics for the inflammation response of PBMCs (cell

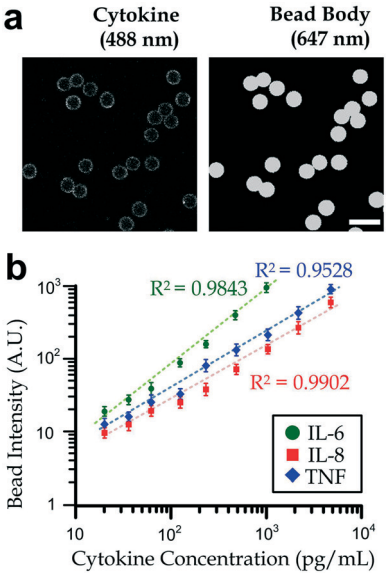

Fig. 4 Cytokine measurement using the microfluidic immunoassay device. (a) Fluorescence micrographs of microbead bodies (647 nm) and cytokine-sensitive intensities (488 nm). Scale bar: 10 μm. (b) Calibration curves for IL-6, IL-8 and TNF measured in the detection microchambers. Note that an intensity below the level of 20 pg ml^{-1} should be considered as negligible for the corresponding cytokine. $N > 100$ from 3 repeated experiments. Error bars represent the standard errors.

density: 3×10^5 cells per ml) following the protocols to incubate and stimulate cells with 1 μl of PHA at a defined concentration (1 μg ml^{-1}, 3 μg ml^{-1} or 5 μg ml^{-1}) as described in the previous sections (Fig. 1b and 3a). Right before the stimulation, one detection microchamber was first used to measure the fluorescence level of the microbead bodies (647 nm) as a reference to determine the optimized exposure time for the following imaging actions. After the PHA stimulation, immune cell secretory cytokine samples were extracted from the culture chamber into three detection microchambers at each of the five selected time points (0 h, 2 h, 4 h, 16 h and 24 h) for the three target cytokines, *i.e.* IL-6, IL-8 and TNF. These time points were chosen carefully based on the typical short-term and long-term cytokine responses as previously reported by other researchers. Kern *et al.* discovered that IL-6 secreted from immune cells in obese patients upon stimulation should increase significantly within 3 h, whereas the TNF level could continue to rise for 24 h. Fong *et al.* reported that IL-8 release of immune cells after stimulation by TGF-β1 could reach a peak level after 16 h.[61] In addition, we also performed the cytokine profiling of PBMCs without PHA stimulation as control. The sample fluorescence micrographs are available in Fig. S3.†

Our results (Fig. 5) show that PHA can stimulate PBMCs to secrete IL-6 and IL-8. However the secretion of TNF was very low as compared to the cytokine secretion without the stimulations. For example, a higher concentration of PHA would induce a more rapid IL-8 secretion, which then stabilized after 24 h at a level ~2.4–2.7 × 10^3 pg ml^{-1}. It is likely that different PHA concentrations might trigger different

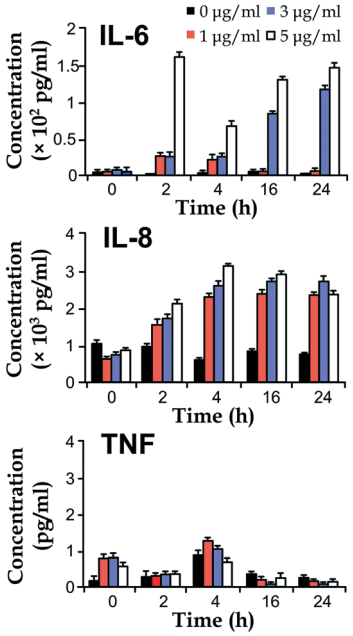

Fig. 5 Dynamic cytokine secretions of IL-6, IL-8 and TNF from PBMCs stimulated by different levels of PHA. The TNF levels are considered to be insignificant as they are below the microbead sensitivity. $N > 100$ from three repeated experiments. Error bars represent the standard errors.

modes of the cytokine secretion profile. Taking the IL-6 response as an example, 1 μg ml^{-1} PHA caused only a short term cytokine secretion up to a level of ~25 pg ml^{-1} within the first 4 h of stimulation, whereas a higher PHA concentration of 3 μg ml^{-1} could induce a longer-term response with a continuous increment of the IL-6 level up to 112 pg ml^{-1} over the 24 h monitoring period. More interestingly, for the PHA concentration of 5 μg ml^{-1}, other than the even higher level of IL-6 secretion than that from the 3 μg ml^{-1} PHA stimulation, we observed a rapid IL-6 secretion (143 pg ml^{-1}) within the first 2 h of stimulation, which might implicate an additional short-term mechanism in the inflammatory response of PBMCs. Moreover, it seems that PHA cannot stimulate TNF secretion of PBMCs (the measured TNF levels are below the 20 pg ml^{-1} sensitivity of the microbeads).

We performed additional experiments to verify the accuracy of the cytokine profiling using the microfluidic immunoassay device by comparing with the conventional flow cytometry. We cultured five wells of PBMCs (3×10^5 cells per ml) with 3 ml of media and applied PHA stimulation (3 μg ml^{-1}) with different durations (0 h, 2 h, 4 h, 16 h and 24 h) before the cytokine quantification. In each measurement, we extracted ~0.1 of the culture media for IL-6 quantification using the microfluidic device, whereas the rest of the media were measured with standard protocols of cytometric fluorescent microbeads with flow cytometry. Results (Fig. S4†) show good agreements between the cytokine levels obtained from the two different detection methods, confirming that the reported microfluidic approach can offer promising cytokine measurements as well as the dynamic cytokine responses of blood cells.

The feasibility of further profiling with more cytokine types and time points is greatly limited by the allowable blood extraction from a human subject, whereas the microfluidic device design can be reconfigured with more detection microchambers without inducing a significant increase in the required biosample volume. Such a sample-sparing approach will enable rapid, on-chip blood assays with a short assay time and small-volume blood collection *via* finger prick. This device may even be implemented for clinical prognosis and diagnosis applications in the near future, considering that some products of the cytometric fluorescent beads were submitted for the Food and Drug Authority (FDA) approval years ago[62] . In addition, there are other detection beads covering a comprehensive collection of cytokines (IL-1β, IL-10, and IL-12p70) available in the market;[12] and hence this device can be applied to unveil characteristics of cytokine secretion dynamics for a broad range of cell and cytokine types for extended cell studies, *e.g.* immune diseases, cancer and stem cell research.[63] Further optimizing the spatiotemporal cytokine measurement technique for multiple cell subpopulation communities or even single immune cells would provide a new set of scientific data for advancing immunology knowledge on intercellular communications as well as cancer immunotherapies.

Further development of this microfluidic technique should include elimination of the microscope in order to induce a standalone system. One potential approach is to adopt a highly sensitive photo-detector for acquiring the average fluorescence level at the detection microchamber. We have studied its feasibility by performing a pilot test for the calibration curve of IL-6-sensitive microbeads (Fig. S5†) based on the average intensity over the microchamber (density: 5×10^3 beads per μl), instead of the individual beads. With the rapid, low-volume, high-sensitivity, and multiplex assay capability and clinical compatibility, the technique holds great promise to advance a medical technology for immune disease control, monitoring, and prevention.

Conclusion

In summary, we developed an integrated microfluidic biosensing platform that can synthesize all the necessary processes for functional cellular immunophenotyping by coupling microfluidic technology with optical biosensing imaging. These include on-chip cell processing, microfluidic multiplexing, active mixing of components and a computer-based control interface for automatic, rapid, and sensitive fluorescent microbead-based cytokine detection from human PBMCs. The new platform will permit high-dimensional immune phenotype profiling (up to 16 tests from one sample) with a much shorter assay time (15–30 min), a smaller amount of sample volume (~0.16 μl for each cytokine test), and a higher sensitivity (20 pg ml^{-1}), which provides a unique advantage over the traditional ELISA-related techniques. The resulting detection system enables both spatial and temporal mapping of cell-secreted cytokine profiles of immune cells at

high throughput and sensitivity. Combining both the spatial and temporal secretion patterns detected with the new microfluidics-based optical biosensing platform would provide a significant signature that quantitatively characterizes the immunophenotypes of patients and would therefore allow for more precise diagnosis and stratification of immune-related diseases.

Conflicts of interest

There are no conflicts to declare.

Acknowledgements

We acknowledge financial support from the National Natural Science Foundation of China (NSFC 31500758), Hong Kong Research Grant Council (GRF 11206014 and 11204317), the City University of Hong Kong (SRG-Fd 7004540), the National Science Foundation (CBET 1701363), New York University Global Seed Grant, and the NYU Clinical and Translational Science Institute Collaborative Translational Pilot Award (NIH/NCATS 1UL1 TR001445).

References

1 G. Pantaleo and A. Harari, *Nat. Rev. Immunol.*, 2006, **6**, 417–423.
2 G. Pantaleo and R. A. Koup, *Nat. Med.*, 2004, **10**, 806–810.
3 C. Ma, R. Fan, H. Ahmad, Q. Shi, B. Comin-Anduix, T. Chodon, R. C. Koya, C.-C. Liu, G. A. Kwong and C. G. Radu, *Nat. Med.*, 2011, **17**, 738–743.
4 P. Chen, N.-T. Huang, M.-T. Chung, T. T. Cornell and K. Kurabayashi, *Adv. Drug Delivery Rev.*, 2015, **95**, 90–103.
5 J. J. O'Shea and P. J. Murray, *Immunity*, 2008, **28**, 477–487.
6 P. Lacy and J. L. Stow, *Blood*, 2011, **118**, 9–18.
7 J. P. Sikora, D. Chlebna-Sokol and A. Krzyzanska-Oberbek, *Arch. Immunol. Ther. Exp.*, 2001, **49**, 399–404.
8 S. M. Opal and V. A. DePalo, *Chest*, 2000, **117**, 1162–1172.
9 W. Chen, N. T. Huang, B. Oh, R. H. Lam, R. Fan, T. T. Cornell, T. P. Shanley, K. Kurabayashi and J. Fu, *Adv. Healthcare Mater.*, 2013, **2**, 965–975.
10 C. C. Czerkinsky, L. A. Nilsson, H. Nygren, O. Ouchterlony and A. Tarkowski, *J. Immunol. Methods*, 1983, **65**, 109–121.
11 Y. Liu, J. Yan, M. C. Howland, T. Kwa and A. Revzin, *Anal. Chem.*, 2011, **83**, 8286–8292.
12 S. X. Leng, J. E. McElhaney, J. D. Walston, D. Xie, N. S. Fedarko and G. A. Kuchel, *J. Gerontol., Ser. A*, 2008, **63**, 879–884.
13 W. Chen, N. T. Huang, X. Li, Z. T. Yu, K. Kurabayashi and J. Fu, *Front. Oncol.*, 2013, **3**, 98.
14 J. S. Boomer, K. To, K. C. Chang, O. Takasu, D. F. Osborne, A. H. Walton, T. L. Bricker, S. D. Jarman 2nd, D. Kreisel, A. S. Krupnick, A. Srivastava, P. E. Swanson, J. M. Green and R. S. Hotchkiss, *JAMA, J. Am. Med. Assoc.*, 2011, **306**, 2594–2605.
15 A. G. Bais, I. Beckmann, P. C. Ewing, M. J. Eijkemans, C. J. Meijer, P. J. Snijders and T. J. Helmerhorst, *Mediators Inflammation*, 2007, **2007**, 24147.
16 W. N. Vreeland, R. J. Meagher and A. E. Barron, *Anal. Chem.*, 2002, **74**, 4328–4333.
17 D. C. Pregibon, M. Toner and P. S. Doyle, *Science*, 2007, **315**, 1393–1396.
18 M. Kunz and S. M. Ibrahim, *Mediators Inflammation*, 2009, **2009**, 979258.
19 D. Payen, G. Monneret and R. Hotchkiss, *Crit. Care*, 2013, **17**, 1.
20 G. Landskron, M. De la Fuente, P. Thuwajit, C. Thuwajit and M. A. Hermoso, *J. Immunol. Res.*, 2014, **2014**, 149185.
21 J. J. O'Shea, C. A. Hunter and R. N. Germain, *Nat. Immunol.*, 2008, **9**, 450–453.
22 S. M. Kaech and E. J. Wherry, *Immunity*, 2007, **27**, 393–405.
23 A. Revzin, E. Maverakis and H. C. Chang, *Biomicrofluidics*, 2012, **6**, 21301–2130113.
24 P. Chen, N. T. Huang, M. T. Chung, T. T. Cornell and K. Kurabayashi, *Adv. Drug Delivery Rev.*, 2015, **95**, 90–103.
25 J.-L. He, A.-T. Chen, J.-H. Lee and S.-K. Fan, *Int. J. Mol. Sci.*, 2015, **16**, 22319–22332.
26 J.-R. Gong, *Small*, 2010, **6**, 967–973.
27 T. M. Squires, R. J. Messinger and S. R. Manalis, *Nat. Biotechnol.*, 2008, **26**, 417–426.
28 P. M. Valencia, P. A. Basto, L. Zhang, M. Rhee, R. Langer, O. C. Farokhzad and R. Karnik, *ACS Nano*, 2010, **4**, 1671–1679.
29 M. Niepel, S. L. Spencer and P. K. Sorger, *Curr. Opin. Chem. Biol.*, 2009, **13**, 556–561.
30 F. Re and J. L. Strominger, *Immunobiology*, 2004, **209**, 191–198.
31 S. J. Altschuler and L. F. Wu, *Cell*, 2010, **141**, 559–563.
32 H.-P. Chou, M. A. Unger and S. R. Quake, *Biomed. Microdevices*, 2001, **3**, 323–330.
33 M. A. Unger, H.-P. Chou, T. Thorsen, A. Scherer and S. R. Quake, *Science*, 2000, **288**, 113–116.
34 M. Junkin, A. J. Kaestli, Z. Cheng, C. Jordi, C. Albayrak, A. Hoffmann and S. Tay, *Cell Rep.*, 2016, **15**, 411–422.
35 R. H. Lam and W. J. Li, *Micromachines*, 2012, **3**, 279–294.
36 T. J. Ober, D. Foresti and J. A. Lewis, *Proc. Natl. Acad. Sci. U. S. A.*, 2015, **112**, 12293–12298.
37 C. Yang, D. Hu, B. Sun, X. Cui, Q. Zhu and R. H. Lam, *Microfluid. Nanofluid.*, 2015, **19**, 711–720.
38 Y.-H. Lin, C.-C. Wang and K. F. Lei, *Biomed. Microdevices*, 2014, **16**, 199–207.
39 C.-C. Lin, J.-H. Wang, H.-W. Wu and G.-B. Lee, *J. Assoc. Lab. Autom.*, 2010, **15**, 253–274.
40 S. Gordon and P. R. Taylor, *Nat. Rev. Immunol.*, 2005, **5**, 953–964.
41 P. Salgame, J. S. Abrams, C. Clayberger, H. Goldstein, J. Convit, R. L. Modlin and B. R. Bloom, *Science*, 1991, **254**, 279–282.
42 J. Yakovleva, R. Davidsson, M. Bengtsson, T. Laurell and J. Emnéus, *Biosens. Bioelectron.*, 2003, **19**, 21–34.
43 F. Y. Lin, M. Sabri, J. Alirezaie, D. Li and P. M. Sherman, *Clin. Diagn. Lab. Immunol.*, 2005, **12**, 418–425.
44 P. Chen, M. T. Chung, W. McHugh, R. Nidetz, Y. Li, J. Fu, T. T. Cornell, T. P. Shanley and K. Kurabayashi, *ACS Nano*, 2015, **9**, 4173–4181.

45 M. Michalzik, R. Wilke and S. Büttgenbach, *Sens. Actuators, B*, 2005, **111**, 410–415.
46 S. Mulvaney, C. Cole, M. Kniller, M. Malito, C. Tamanaha, J. Rife, M. Stanton and L. Whitman, *Biosens. Bioelectron.*, 2007, **23**, 191–200.
47 C. Lim and Y. Zhang, *Biosens. Bioelectron.*, 2007, **22**, 1197–1204.
48 A. H. Ng, U. Uddayasankar and A. R. Wheeler, *Anal. Bioanal. Chem.*, 2010, **397**, 991–1007.
49 R. Chaerkady and A. Pandey, *Annu. Rev. Pathol.: Mech. Dis.*, 2008, **3**, 485–498.
50 H. Y. Hsu, T. O. Joos and H. Koga, *Electrophoresis*, 2009, **30**, 4008–4019.
51 Y. Tang, C. Liao, X. Xu, H. Song, S. Shi, S. Yang, F. Zhao, W. Xu, X. Chen and J. Mao, *Clin. Microbiol. Infect.*, 2011, **17**, 1666–1673.
52 E. M. Carvalho, O. Bacellar, A. F. Porto, S. Braga, B. Galvão-Castro and F. Neva, *JAIDS, J. Acquired Immune Defic. Syndr.*, 2001, **27**, 1–6.
53 H. Bonig, H. Laws, A. Wundes, J. Verheyen, M. Hannen, Y. Kim, U. Banning, W. Nurnberger and D. Korholz, *Bone Marrow Transplant.*, 2000, **26**, 91–96.
54 R. H. Lam, X. Cui, W. Guo and T. Thorsen, *Lab Chip*, 2016, **16**, 1652–1662.
55 J. H. Cox, G. Ferrari and S. Janetzki, *Methods*, 2006, **38**, 274–282.
56 S. C. Johnson, D. J. Marshall, G. Harms, C. M. Miller, C. B. Sherrill, E. L. Beaty, S. A. Lederer, E. B. Roesch, G. Madsen, G. L. Hoffman, R. H. Laessig, G. J. Kopish, M. W. Baker, S. A. Benner, P. M. Farrell and J. R. Prudent, *Clin. Chem.*, 2004, **50**, 2019–2027.
57 D. A. Beard, *J. Appl. Phys.*, 2001, **89**, 4667–4669.
58 X. Cui, H. M. Yip, Q. Zhu, C. Yang and R. H. W. Lam, *RSC Adv.*, 2014, **4**, 16662–16673.
59 J. Fucikova, I. Moserova, I. Truxova, I. Hermanova, I. Vancurova, S. Partlova, A. Fialova, L. Sojka, P. F. Cartron and M. Houska, *Int. J. Cancer*, 2014, **135**, 1165–1177.
60 G. Y. Lee and C. T. Lim, *Trends Biotechnol.*, 2007, **25**, 111–118.
61 C. Y. Fong, L. Pang, E. Holland and A. J. Knox, *Am. J. Physiol.*, 2000, **279**, L201–L207.
62 E. Morgan, R. Varro, H. Sepulveda, J. A. Ember, J. Apgar, J. Wilson, L. Lowe, R. Chen, L. Shivraj and A. Agadir, *Clin. Immunol.*, 2004, **110**, 252–266.
63 E. K. Sackmann, A. L. Fulton and D. J. Beebe, *Nature*, 2014, **507**, 181–189.